Structure of the sulfur *K* x-ray emission spectrum: influence of the oxidation state

2012 J. Phys. B: At. Mol. Opt. Phys. 45 025004

(http://iopscience.iop.org/0953-4075/45/2/025004)

J. Phys. B: At. Mol. Opt. Phys. **45** (2012) 025004 (10pp) doi:10.1088/0953-4075/45/2/025004

Structure of the sulfur *K* x-ray emission spectrum: influence of the oxidation state

P D Pérez, A C Carreras and J C Trincavelli

Instituto de Física Enrique Gaviola (IFEG)—CONICET, Facultad de Matemática, Astronomía y Física, Universidad Nacional de Córdoba, Medina Allende s/n, Ciudad Universitaria, 5016 Córdoba, Argentina

E-mail: trincavelli@famaf.unc.edu.ar

Received 5 September 2011, in final form 11 November 2011
Published 9 January 2012
Online at stacks.iop.org/JPhysB/45/025004

Abstract

The sulfur *K* x-ray emission was studied in pure sulfur, anhydrite ($CaSO_4$) and sphalerite (ZnS) samples. The ionizations were induced by electron impact and the spectra were recorded with a wavelength dispersive spectrometer. The spectral processing was performed through a methodology based on the optimization of atomic and experimental parameters. Energies and intensities of diagram and satellite lines were determined for a set of transitions in the $K\alpha$ and $K\beta$ groups. The lines studied include $K\alpha_{22}$, $K\alpha_2$, $K\alpha_1$, $K\alpha'$, $K\alpha_3$, $K\alpha_4$, $K\alpha_5$, $K\alpha_6$, $K\beta_{1,3}$, $K\beta$-RAE, $K\beta^{III}$, $K\beta^{IV}$, $K\beta_x$, $K\beta'$ and $K\beta''$. The main spectral differences between the three oxidation states were analysed, considering the influence of the ligand atoms. The results were compared with data published by other authors and the origin of certain lines was discussed on the basis of data available in the literature.

1. Introduction

The x-ray emission in atomic transitions from inner-shell hole states to more stable configurations is the mechanism that leads to the energy balance in some atomic relaxation processes. The fine structure features of the x-ray emission spectra contain valuable information about the existence and nature of some atomic processes and about the influence of molecular effects. In addition, certain differences in the characteristics of diagram and satellite lines observed between pure elements and compounds are typically attributed to the chemical bonds. For these reasons, there is an increasing interest in the study of the *K* satellite lines appearing in the x-ray spectra of elements of the third and fourth periods.

Several processes have been attributed to the emission of the different kinds of *K* satellite lines, such as multiple ionization [1–13], exchange interaction [14], plasmon excitation [15–17], radiative Auger effect [1, 18–27] and molecular orbitals [28, 29]. On the other hand, the structure of the characteristic x-ray spectrum emitted by an element is influenced by the chemical environment of the corresponding atoms. This influence is more important in the $K\beta$ region than in the $K\alpha$ region, since $K\beta$ lines arise from transitions involving the 3p shell, which is more external than the 2p shell related to the $K\alpha$ lines. The theory of molecular orbitals has been successfully applied to explain the distortion of x-ray spectra due to chemical bondings in elements of the third period [30–32], whereas for compounds involving elements of the fourth period, the change in the spectral structure was attributed to 3p3d exchange interaction [33, 34] and charge transfer effects [35].

The relative intensities, natural linewidths and characteristic energies of the diagram, forbidden and satellite $K\beta$ lines emitted by an element depend on the oxidation state of the corresponding atoms. Moreover, some transitions can occur only in compounds and they are not observed in pure elements. In the $K\alpha$ region, although the influence of chemical bondings is not so important, some variations in the relative intensities and some slight energy shifts of the whole group were observed as a consequence of the chemical environment [36]. The knowledge of these parameters and their dependence on the oxidation state are a key for a better understanding of intra-atomic electron correlation, excitation dynamics, relaxation and other atomic [6, 7, 37–43] and molecular [28, 29] effects.

Thus, for example, for elements of the third period, a detailed knowledge of the *K*-line emission spectrum is of interest due to its application to chemical speciation. In some situations, it provides information about the degree of reactivity of the considered element with the environment. In the particular case of sulfur, the information about certain transitions is scarce or not available in the literature.

Particularly, a full study of the sulfur K x-ray emission induced by electron incidence has not been performed to date, despite its interest in environmental [31, 44–46] and geological [36, 47] applications.

The spectral structure of the elements of the third period involves several lines that can be grouped into two regions: $K\alpha$ and $K\beta$. In the first region, the $K\alpha_1$ and $K\alpha_2$ diagram lines can be observed along with the $K\alpha_{22}$, $K\alpha'$, $K\alpha_3$, $K\alpha_4$, $K\alpha_5$ and $K\alpha_6$ satellites. The $K\alpha'$, $K\alpha_3$ and $K\alpha_4$ lines are associated with double-ionization processes and to the subsequent modification of the atomic energy levels due to a spectator hole in the L shell; these transitions are usually denoted as $K\alpha L^1$ lines. Similarly, $K\alpha_5$ and $K\alpha_6$ lines are referred to as $K\alpha L^2$ lines, because they are originated by decays produced in the presence of two spectator holes in the L shell. The processes responsible for the creation of spectator holes are the so-called shake-off, shake-up, two-step-one (or TS1, in which the electron ejected after the first collision pulls out another bound electron of the same atom) and two-step-two (or TS2, in which the incident electron creates sequentially two vacancies) [38]. The $K\alpha_{22}$ satellite line is produced by a radiative Auger emission KLM, in which the atom is also doubly ionized [37].

As previously mentioned, the $K\beta$ region of the sulfur spectrum depends significantly on the oxidation state. Besides the main $K\beta_{1,3}$ peak, several satellite lines can be observed: $K\beta'$, a KMM radiative Auger emission, $K\beta''$, $K\beta^{\mathrm{III}}$ and $K\beta^{\mathrm{IV}}$. For pure sulfur, the main $K\beta_{1,3}$ transition corresponds to a doublet formed by two lines due to molecular orbitals which relate different levels of the S_8 molecule [48], while in oxides, it is associated with a transition from a molecular orbital composed of the $S3$p and $O2$p atomic orbitals to the $S1$s orbital, where S denotes the sulfur atom and O the oxygen atom. The $K\beta'$ line can be explained by the transition from a molecular orbital built of $S3$p and $O2$s atomic orbitals to the $S1$s orbital. Thus, the difference between the $K\beta_{1,3}$ and $K\beta'$ transitions arises from the atomic orbital of the ligand involved. For this reason, the corresponding energy difference is approximately given by the difference between the energies of the 2s and 2p orbitals of the ligand, which is 15 eV in the case of oxygen [31].

According to different authors [49, 50] a line denoted by $K\beta_{\mathrm{x}}$ associated with a decay from a molecular orbital formed by $S3$s and $O2$s orbitals appears a few eV below the main $K\beta_{1,3}$ line. This structure has also been attributed to a KMM radiative Auger emission for other elements of the third period [38], but the origin of this line is still unclear. Regarding the $K\beta''$ line appearing at the high-energy side of the $K\beta$ group, it corresponds to a transition from a molecular orbital involving the $O2$p, $S3$p and $S3$s atomic orbitals [31].

The interpretation of the $K\beta^{\mathrm{III}}$ and $K\beta^{\mathrm{IV}}$ lines is more straightforward. Their origin is related to a modification of the atomic levels in the presence of a $2p$ spectator hole. Due to the scarcity of data about the intensity of these lines and the greater availability of data for $K\alpha_{3,4}$ lines, the search for a relationship between them is of interest. Nevertheless, the assumption that $K\alpha$ and $K\beta$ emission probabilities are unaffected by the presence of a spectator hole, i.e. that $K\alpha_{3,4}/K\alpha$ and $K\beta^{\mathrm{III,IV}}/K\beta$ ratios are similar, is a very rough approximation.

In this work, the structure of the sulfur K-line emission spectrum was studied in samples with sulfur in different oxidation states; particularly, characteristic energies and transition probabilities (RTP) relative to all the decays from L ($K\alpha$) or M ($K\beta$) shells were determined. With this purpose, x-ray emission spectra induced by electron incidence were measured for pure sulfur, anhydrite ($CaSO_4$) and sphalerite (ZnS) by means of a wavelength dispersive spectrometer (WDS) attached to a scanning electron microscope (SEM). The spectra obtained were fitted with a homemade software developed for spectral processing based on a method for the refinement of experimental and atomic parameters [51, 52]. This method considers in detail the interaction processes of electrons and x-rays within the sample, and the interaction of the emitted x-rays with the detector. The atomic parameters obtained were analysed and compared with data from the literature (when available) for different compounds. In addition, the behaviour of certain parameters with the atomic number was studied, complementing with results from previous publications [37, 38].

2. Experiment and fitting procedure

Pure sulfur and anhydrite ($CaSO_4$) samples were prepared for the measurement of sulfur K x-ray emission induced by electron incidence. In addition, a sphalerite (ZnS) sample from the SPI #2753 reference standard set was used. The three samples were carbon coated due to their low electric conductivity. The measurements were performed with an INCA Wave 700 WDS attached to a LEO 1450VP SEM from the Laboratorio de Microscopía Electrónica y Microanálisis (LABMEM) of the Universidad Nacional de San Luis (UNSL), Argentina. Both $K\alpha$ and $K\beta$ sulfur spectra were obtained with a PET (pentaerythrite) analyser crystal in Johansson geometry. The energy of the $K\alpha_1$ line given by Bearden [53] for pure sulfur (2.307 84 keV) was used as a reference for the calibration of the spectrometer. Beam currents and measuring times are summarized in table 1. The collimator slit size (0.50 mm) and the beam current were chosen to obtain a compromise solution between a good energy resolution and high counting statistics, minimizing sample damage. For instance, the instrumental resolution (FWHM) and counting rate of the most intense peak ($K\alpha_{1,2}$ of pure sulfur) were 2 eV and 70 000 counts s^{-1}, respectively. The samples were excited by a 20 keV electron beam and the spectra were measured at a 29° take-off angle.

Due to the requirement of high dose deposition in the samples, the possible effect of surface charge accumulation was analysed. Thus, the pure sulfur spectrum was processed with incidence energies lower than the nominal one down to 15 keV, in order to simulate the effect of electron stopping because of the charge accumulated in the sample. No effect could be observed in the atomic parameters studied.

The spectral processing was performed by means of a method previously developed and implemented in the software POEMA [51, 52]. This method consists in minimizing the differences between the experimental spectrum and an analytical function proposed to describe it by means of

Table 1. Average beam current and time for measuring the sample spectra. Numbers in parentheses indicate the estimated uncertainties in the last digit.

	$K\alpha$ spectra			$K\beta$ spectra		
Sample	Average beam current (nA)	Measuring time (min)	Interval (keV)	Average beam current (nA)	Measuring time (min)	Interval (keV)
Sphalerite	83.6(2)	8	2.2936 2.3366	84.1(4)	13	2.4380 2.5169
Pure sulfur	104.9(2)	16	2.2919 2.3483	105.4(5)	15	2.4313 2.5304
Anhydrite	83.3(1)	8	2.2936 2.3366	83.9(1)	13	2.4378 2.5169

the optimization of a set of parameters involved in the analytical description. This function takes into account all the physical processes that can occur in the sample and in the detector, and that contribute to the spectrum: the emission of characteristic lines and bremsstrahlung, x-ray absorption, fluorescence enhancement [54] and the detector efficiency [55]. A Voigt profile [56] was used to describe the shape of each emission line, with the exception of the $K\beta_{1,3}$ line for which two Voigt functions were necessary. The choice of the function that describes the line profiles is very important because it markedly influences on the areas and widths of the peaks, and consequently, on the transition probabilities obtained for the corresponding lines. A Voigt function is a convolution of a Gaussian, which properly describes the instrumental broadening, and a Lorentzian, which is associated with the natural width of the characteristic lines. In addition, two satellite bands related to radiative Auger transitions, and described by Gaussian profiles, were considered in the $K\beta$ spectrum of pure sulfur. These structures were observed at the low energy side of the main $K\beta_{1,3}$ line. The $K\beta^{\mathrm{III}}$ and $K\beta^{\mathrm{IV}}$ transitions were not observed for anhydrite because the statistics was not good enough in the corresponding spectral region.

Characteristic energies, relative transition probabilities (RTP) and natural linewidths were obtained as a result of the spectral fitting procedure, along with some experimental parameters. During the optimization procedure, certain constraints were imposed due to their physical meaning. Thus, the relative intensity R_1 corresponding to the $K\alpha_1$ line and satellite lines associated with $L_3 \rightarrow K$ transitions was forced by an iterative process to coincide with the corresponding R_1^{theor} ratio predicted by Scofield for single ionization [57]. This procedure was carried out by taking into account that the relative intensity R_1 has two contributions: the relative intensity R_1^{exp} associated with the main $K\alpha_1$ line, and the fraction corresponding to the satellite lines. If it is assumed that the presence of spectator holes do not modify the probability of a particular decay (from L_2 or L_3) to the K shell, that fraction can be calculated as the product $R_1^{\mathrm{theor}}\, R_{\mathrm{sat}}^{\mathrm{exp}}$, where the second factor is the relative intensity of all the satellite transitions in the $K\alpha$ group. Therefore,

$$R_1 = R_1^{\mathrm{exp}} + R_1^{\mathrm{theor}} R_{\mathrm{sat}}^{\mathrm{exp}}. \qquad (1)$$

3. Results and discussion

Figure 1 shows some of the measured spectra along with their corresponding fits, as examples. The $K\alpha$ spectral region does not exhibit important differences among the sulfur species (except for the $K\alpha L^1$ region, see table 2). For this reason, this spectral region is shown only for pure sulfur (see figure 1(a)). The $K\beta$ group, however, shows significant differences in energy, intensity and width for some peaks of different species (see figures 1(b)–(d)). Moreover, certain lines can be observed only for some of the species studied (e.g. $K\beta'$ in anhydrite). The energy resolution of the spectrometer used in the measurements allowed us to separate the $K\alpha_3$, $K\alpha_4$, $K\alpha_5$, $K\alpha_6$, $K\beta^{\mathrm{III}}$ and $K\beta^{\mathrm{IV}}$ lines, and to fit them as single lines (see tables 2 and 3). However, in the analysis of results they were grouped in doublets for comparison with data from the literature. To this end, the energy of the doublet was considered as the intensity-weighted average of both energies, and the corresponding intensity was taken as the sum of the intensities.

The uncertainties of the results were estimated by error propagation of the uncertainties of the intensities registered by the spectrometer for all the channels, which were regarded as stochastic variables, with standard deviations given by the square roots of the mean values.

3.1. Kα group

The characteristic energies obtained from the spectral processing of the S-$K\alpha$ region are presented in table 2 along with the corresponding RTP for pure sulfur, sphalerite and anhydrite.

3.1.1. $K\alpha_1$ and $K\alpha_2$ diagram lines. The $K\alpha_1$ and $K\alpha_2$ diagram lines, corresponding to $L_3 \rightarrow K$ and $L_2 \rightarrow K$ decays, respectively, are the main transitions in the $K\alpha$ group. These peaks are properly described by Voigt functions, as can be seen in figure 1(a). Energy shifts of these peaks were observed for different oxidation states. As shown in table 2, the $K\alpha_1$ line moves 0.5 eV towards lower energies for sphalerite (S^{-2}), whereas it moves 0.8 eV towards higher energies for anhydrite (S^6). In addition, the same trend was observed for all the transitions studied (see table 2). All the sulfur $K\alpha$ lines measured in sphalerite have energies between 0.4 and 0.6 eV lower than that corresponding to pure sulfur, while in anhydrite

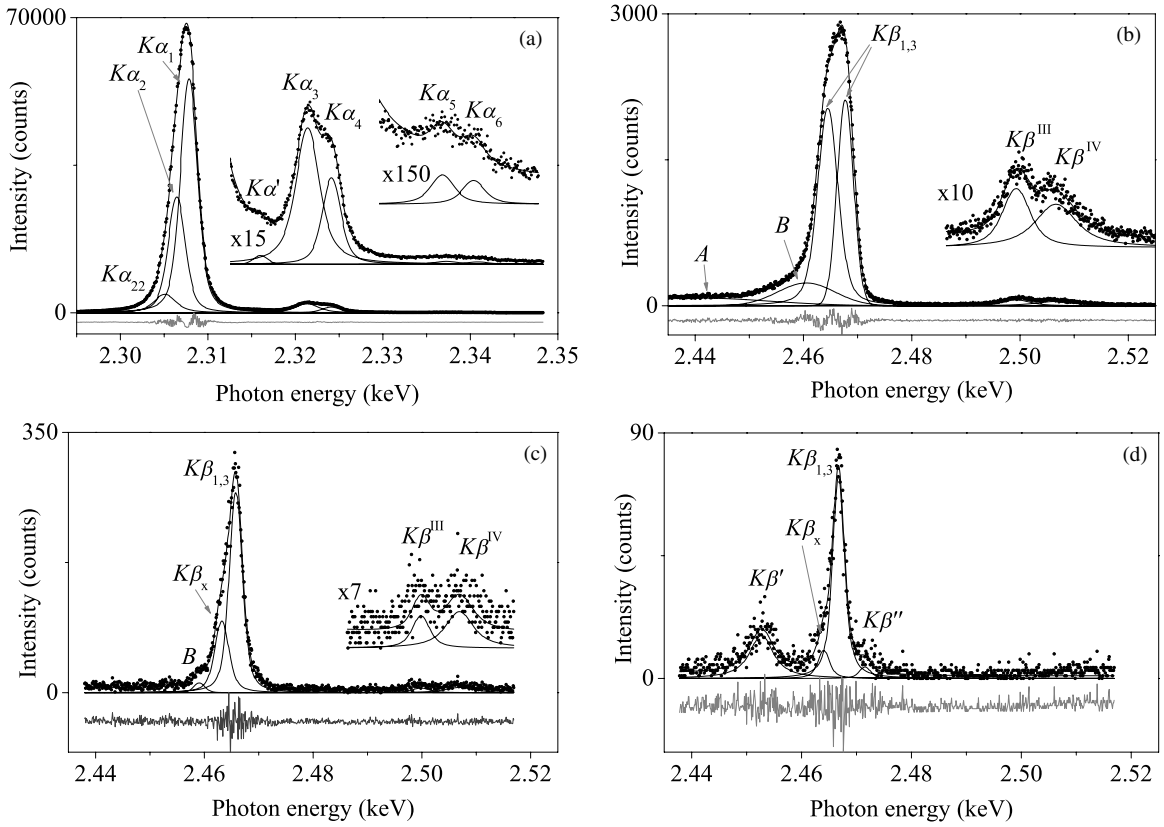

Figure 1. Some of the measured spectra: (a) pure sulfur—$K\alpha$ zone, (b) pure sulfur—$K\beta$ zone, (c) sphalerite—$K\beta$ zone, (d) anhydrite—$K\beta$ zone. The insets show amplified views of low intensity regions.

Table 2. Energies and transition probabilities of the S-$K\alpha$ lines for pure sulfur and sulfur-based compounds. Numbers in parentheses indicate the estimated uncertainties in the last digit.

	ZnS (S^{-2})		Pure S (S^0)		$CaSO_4$ (S^6)	
Transition	Energy (keV)	RTP	Energy (keV)	RTP	Energy (keV)	RTP
$K\alpha_{22}$	2.3046(5)	0.063(4)	2.305 19(5)	0.074(1)	2.3060(6)	0.085(4)
$K\alpha_2$	2.306 06(2)	0.2909(5)	2.306 46(2)	0.2885(6)	2.307 39(4)	0.276(3)
$K\alpha_1$	2.307 35(1)	0.5931(5)	2.307 84(1)	0.585(3)	2.308 64(1)	0.573(4)
$K\alpha'$	2.3155(6)	0.0015(7)	2.3159(4)	0.0010(3)	2.3173(9)	0.002(1)
$K\alpha_3$	2.3211(7)	0.029(2)	2.3213(1)	0.0346(8)	2.3223(3)	0.041(5)
$K\alpha_4$	2.323 63(7)	0.023(1)	2.324 07(4)	0.0157(5)	2.3251(1)	0.023(5)
$K\alpha_5$			2.3373(9)	0.0007(2)		
$K\alpha_6$			2.3409(8)	0.0005(1)		

Table 3. Energies and transition probabilities of the S-$K\beta$ lines for pure sulfur and sulfur-based compounds. Numbers in parentheses indicate the estimated uncertainties in the last digit.

	ZnS (S^{-2})		Pure S (S^0)		$CaSO_4$ (S^6)	
Transition	Energy (keV)	RTP	Energy (keV)	RTP	Energy (keV)	RTP
RAE KM_1M_1[a]			2.4407(8)	0.09(1)		
RAE $KM_{2,3}M_{2,3}$[b]	2.459(2)	0.023(6)	2.4605(4)	0.11(1)		
$K\beta_{1,3}$-1	2.465 79(2)	0.60(1)	2.464 49(6)	0.41(3)	2.466 72(9)	0.6(1)
$K\beta_{1,3}$-2			2.467 73(2)	0.30(2)		
$K\beta^{III}$	2.4998(2)	0.05(1)	2.4993(2)	0.042(5)		
$K\beta^{IV}$	2.5069(6)	0.09(1)	2.5066(3)	0.049(5)		
$K\beta'$					2.4527(2)	0.28(1)
$K\beta_x$	2.463(2)	0.24(1)			2.464(3)	0.1(1)
$K\beta''$					2.4716(6)	0.07(4)

[a] Peak *A* in figure 1(b). [b] Peak *B* in figure 1(b).

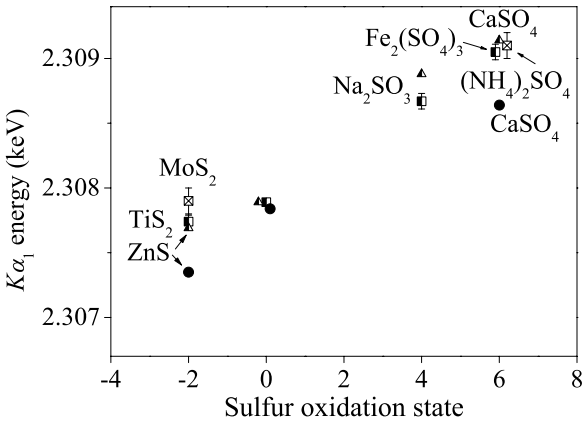

Figure 2. Sulfur $K\alpha_1$ absolute energy versus oxidation state. The point shape indicates the excitation source: electrons (circles), photon (triangles) and protons (squares). Solid circles: present results; half-filled squares: [44]; crossed squares: [59]; half-filled triangles: [60]. Uncertainties in the present results are around the point size.

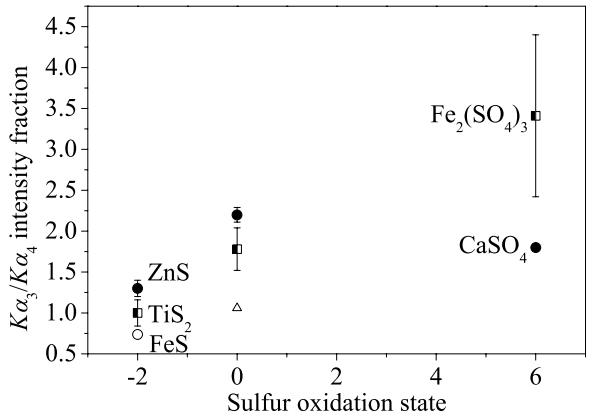

Figure 3. Sulfur $K\alpha_3/K\alpha_4$ intensity ratio versus oxidation state. The point shape indicates the excitation source: photons (triangles), electrons (circles) and protons (squares). Filled circles: present results; empty circles: [62]; empty triangles [41]; half-filled squares: [44].

they are between 0.8 and 1 eV higher than in pure sulfur, with the exception of $K\alpha'$, whose increment is 1.4 eV. The whole effect observed can be described as a global shift to higher energies when increasing the sulfur oxidation state. Earlier publications show the use of this empirical fact for the chemical speciation of sulfur in geological samples. For example, some authors [47, 58] performed a Gaussian fit to the $K\alpha_{1,2}$ doublet and they found a similar trend of the energy shift with the sulfur oxidation state. In this work, the careful spectral processing performed through the method mentioned above, allowed us to obtain absolute energy values for the $K\alpha_1$ lines. In figure 2, the present results are compared with the scarce data available in the literature [44, 59, 60]. As can be seen, for all the data shown in the figure, the characteristic energy increases linearly with the oxidation state. This behaviour could be interpreted bearing in mind that the atomic radius increases with the oxidation state, thus increasing the difference between the energies of the K and L shells, and therefore, displacing the $K\alpha_1$ lines to the higher energy side of the spectrum.

3.1.2. $K\alpha_{22}$ line. As can be seen in figure 1(a), there is a structure appearing at the low energy side of the $K\alpha_2$ line, labelled as $K\alpha_{22}$. For elements with $Z > 20$, several authors have attributed this structure to radiative Auger transitions [26, 27, 61]. For sulfur ($Z = 16$), according to Scofield's calculations [54], the total production of multivacancy states relative to single K vacancy production must be 9.5%. This value should be renormalized with respect to the whole $K\alpha$ group to allow for the comparison with our results. Then, the production of multivacancy states represents the 8.7% of the total (single and multiple) vacancy production. This value is in agreement with our result for the $K\alpha_{22}$ line intensity (which is the 7.4% of the $K\alpha$ group), bearing in mind that *KMM* transitions are not involved in the $K\alpha_{22}$ structure, whereas the calculations performed by Scofield involves *KLL*, *KLM* and also *KMM RAE* contributions. This comparison with theoretical values supports the hypothesis that $K\alpha_{22}$ is originated by multiple vacancy states.

3.1.3. $K\alpha L^1$ satellite lines. The sulfur $K\alpha_3/K\alpha_4$ intensity ratios for the three oxidation states studied (S^{-2}, S^0 and S^6) are presented in figure 3, together with data published by Kavčič *et al* [44] for proton impact, by Mauron *et al* [41] for photon impact and by Parrat [62] for electron impact. It is well known that the probability of double ionization induced by proton impact is higher than by electron impact, which in turn is higher than for photon incidence; particularly, TS2 processes are not possible for photons. This fact explains the dependence of the intensity of $K\alpha L^1$ satellite lines with the excitation source. Indeed, for the transition probability of the whole $K\alpha L^1$ group relative to the $K\alpha$ spectrum, values between 0.013 [63] and 0.044 [64] have been reported for photons, between 0.050 (present results) and 0.068 [62] for electrons, and the value 0.081 [44] for protons. Nevertheless, the behaviour of the $K\alpha_3/K\alpha_4$ ratio with the oxidation state for the different excitation sources cannot be inferred from the double ionization probabilities. In fact, it can be seen in figure 3 that the $K\alpha_3/K\alpha_4$ ratio behaves differently for protons than for electrons, as a function of the oxidation state. Particularly, for S^{-2} this ratio is significantly different than for S^0. This fact could be important for chemical speciation (because other $K\alpha$ parameters present small differences between these states), even though the $K\beta$ region is clearly more sensitive to the oxidation state.

Finally, the $K\alpha'$ peak was also detected (see figure 1(a)) and its energy and intensity were determined (see table 2), although the transition probability is one order of magnitude lower than that corresponding to the other $K\alpha L^1$ satellite lines.

3.1.4. $K\alpha L^2$ satellite lines. Due to the careful spectral processing performed, the weak $K\alpha_5$ and $K\alpha_6$ lines were also analysed for pure sulfur, despite the low counting rate achieved in the measurement of the corresponding spectral region (see figure 1(a)). The energies and transition probabilities were quantified, and the results are presented in table 2. These results were not compared with previous data because they were not found in the literature.

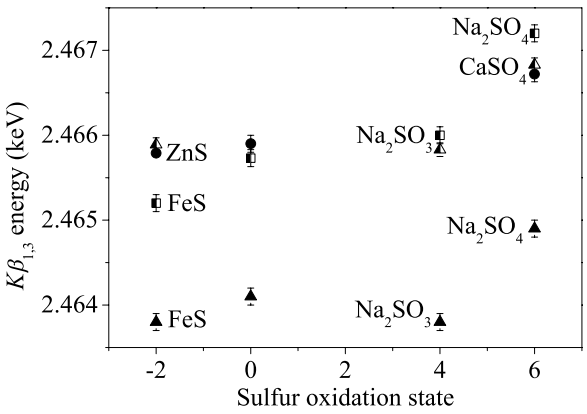

Figure 4. Sulfur $K\beta_{1,3}$ absolute energy versus oxidation state. The point shape indicates the excitation source: electrons (circles), protons (squares) and photons (triangles). Solid circles: present results; solid triangles: [31]; half-filled triangles: [65]; half-filled squares: [48].

3.2. $K\beta$ group

The characteristic energies of the S-$K\beta$ lines and the corresponding RTP, obtained for pure sulfur, sphalerite and anhydrite, are presented in table 3.

3.2.1. $K\beta_{1,3}$ diagram line. Although the sulfur $K\beta$ spectrum is more sensitive to the oxidation state than the $K\alpha$ one, presenting more noticeable changes among different compounds, displacements greater for $K\alpha_1$ than for $K\beta_{1,3}$ were observed (see figures 2 and 4). The maximum energy shift (obtained between S^{-2} and S^6) for $K\alpha_1$ is 1.30 eV while for $K\beta_{1,3}$ it is 0.93 eV.

According to Kavčič *et al* [48], the $K\beta_{1,3}$ transition of pure sulfur is composed of two narrow lines, each of which is originated in an S_8 molecular orbital. The present measurements revealed this structure consisting of two peaks of similar intensities separated 3.2 eV (or 2.5 eV according to Kavčič *et al* [48]) as can be seen in figure 1(b) and table 3. The energy of the S^0-$K\beta_{1,3}$ line shown in figure 4 is the intensity-weighted average of both energies.

On the other hand, in both sphalerite and anhydrite spectra, the main $K\beta_{1,3}$ peak was properly described by a single line. In the case of anhydrite, it has been attributed to a transition from a molecular orbital mainly consisting of *S*3p and *O*2p [31].

3.2.2. $K\beta$ RAE processes and $K\beta_x$ satellite line. Several effects contribute to the structure present in the low energy side of the $K\beta_{1,3}$ peak. The importance of these effects depends on the atomic number and on the oxidation state. In this work, the spectral features of this energy region were analysed for pure sulfur (S^0), sphalerite (S^{-2}) and anhydrite (S^6). Notable differences can be appreciated between the spectra corresponding to different oxidation states (see figures 1(b)–(d)).

For pure sulfur, two broad bands were detected. Their origins are associated with radiative Auger emissions (RAE), in which an Auger electron and a photon share the transition energy. The assignation of a *KMM*-specific transition to each of these bands is not direct. According to Chung and Jenkins [66], the highest possible energy of the outgoing photon can be expressed as

$$E_e = E(K,Z) - 0.5 \times (E(M_i,Z) + E(M_j,Z)) \\ -0.5(E(M_i,Z+1) + E(M_j,Z+1)), \quad (2)$$

where $E(K, Z)$ and $E(M_q, Z)$ are the K and M_q shell-binding energies for the element Z, respectively. For $M_i = M_{2,3}$ and $M_j = M_{2,3}$, (2) can be written as

$$E_e = E(K\beta_{1,3}, S) - E(M_{2,3}, Cl), \quad (3)$$

where $E(K\beta_{1,3}$,S) is the characteristic energy of the $K\beta_{1,3}$ transition for sulfur and $E(M_{2,3}$, Cl) is the $M_{2,3}$ shell binding energy for chlorine. Thus, E_e corresponds to the RAE energy when the Auger electron is ejected from the $M_{2,3}$ shell with zero kinetic energy. From (3), it can be deduced that the energy difference between a radiative Auger emission and the main $K\beta_{1,3}$ line cannot overcome the $-E(M_{2,3}$, Cl) edge; moreover, the RAE peak maximum E_m must be close to this value, because the highest energy E_e almost coincides with the most probable RAE transition. Taking this example into account, by comparison with the band maximum energy obtained from the spectral analysis, the specific shell from which the Auger electron is ejected can be determined. In the case of the structure denoted as *B* in figure 1(b), the difference between E_m and $E(K\beta_{1,3})$ is $\Delta E_B = -5.4 \pm 0.4$ eV, while the $M_{2,3}$ absorption edge for chlorine is 6.8 eV [67]. It must be mentioned that the $M_{4,5}$ shell is not occupied in the ground state of sulfur; in addition, if in (2), the transition $KM_1M_{2,3}$ is considered, the energy value that can not be overcome is 16.05 eV [67], which is too far from ΔE_B. Therefore, it can be assumed that structure *B* is associated with $KM_{2,3}M_{2,3}$ radiative Auger processes. A second RAE band can be attributed to the structure appearing 25.2 ± 0.8 eV below the main $K\beta_{1,3}$ peak and denoted as *A* in figure 1(b). This band can be associated with KM_1M_1 radiative Auger emissions. In fact, by using (2) and the fact that $E(K\beta_{1,3}$,S) = E(*K*,S) – $E(M_{2,3}$,S), it can be easily seen that the difference between E_m and $E(K\beta_{1,3})$ must be close to $E(M_{2,3}$,S) – $E(M_1$,S) – $E(M_1$,Cl) = −25.3 eV.

In the sphalerite spectrum, significant differences with respect to the pure sulfur spectrum can be observed (see figure 1(c)). The structure *A* does not appear, while *B* is narrower, less intense and slightly shifted to the low energy side. The relative intensity of the structure *B* is around 25% of the value corresponding for pure sulfur. Besides, the energy difference between structure *B* and the main $K\beta_{1,3}$ peak is 7 eV (see table 3) which means that this structure can also be assigned to $KM_{2,3}M_{2,3}$ radiative Auger emissions.

Regarding the anhydrite spectrum, a small peak appears at the $K\beta_{1,3}$ low energy tail (see figure 1(d)). This peak is too close to the main line to be associated with a RAE band. According to Torres Deluigi and Riveros [31], this structure, denoted as $K\beta_x$, for several sulfate samples, can be properly described as a transition from a molecular orbital mainly composed of *S*3s and *O*2s atomic orbitals. Since the energy shift determined for the peak (around 3 eV, see table 3) agrees with the value obtained in [31], it is reasonable to assign this peak to the $K\beta_x$ transition. On the other hand, the sphalerite

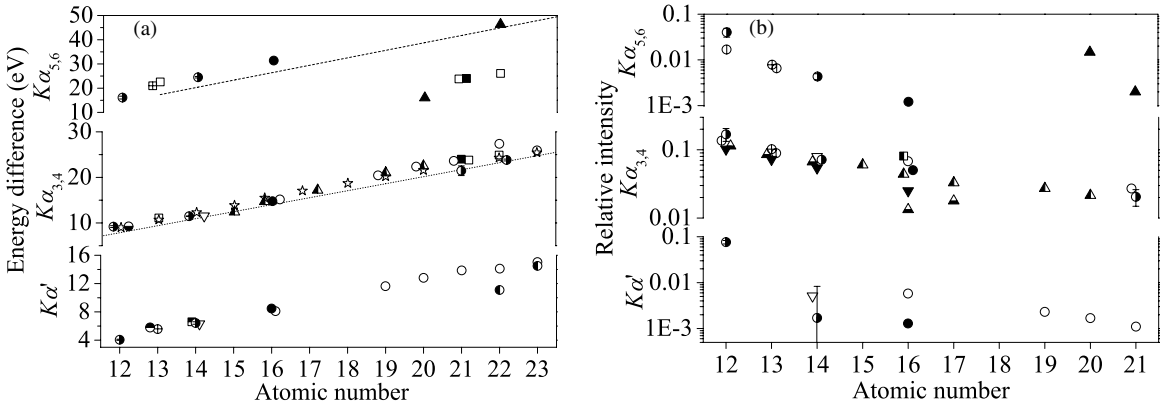

Figure 5. Energies (a) and intensities (b) of $K\alpha'$, $K\alpha_{3,4}$ and $K\alpha_{5,6}$ lines relative to $K\alpha_{1,2}$ versus atomic number. The data denoted by open circles correspond to sulfur compounds. The point shape indicates the excitation source: electrons (circles), protons and heavy ions (squares) and photons (triangles). $E(K\alpha_{5,6})$: solid circles: present results; right-half-filled circles: [37]; filled up triangles: [18]; crossed squares: [69]; empty squares: [70]; solid squares: [2]; dashed line: [71]. $E(K\alpha_{3,4})$: solid circles: present results; right-half-filled circles: [37]; down-half-filled circles: [6]; open circles: [62]; open stars: theoretical data given by [72]; open triangles: [73]; left-half-filled triangles: [64]; open squares: [70]; solid squares: [2]. $E(K\alpha')$: solid circles: present results; right-half-filled circles: [37]; up-half-filled circles: [74]; left-half-filled circles: [75] ($Z = 22$ and 23); crossed circles: [5]; open circles: [62]; open triangles: [73]; and up-half-filled squares: [76]. $I(K\alpha_{5,6})$: solid circles: present results; right-half-filled circles: [37]; vertical strikethrough circles: [71]; crossed circles: [5]; and solid triangles: [18]. $I(K\alpha_{3,4})$: solid circles: present results; right-half-filled circles: [37]; vertical strikethrough circles: [6]; crossed circles: [5]; open circles: [62]; solid triangles: [41]; down-half-filled triangles: [63]; open triangles: [73]; and left-half-filled triangles: [64]. $I(K\alpha')$: solid circles: present results; right-half-filled circles: [37]; open triangles: [73]; open circles: [62].

spectrum exhibits a peak at the same energy (also referred to as $K\beta_x$, see figure 1(c) and table 3), despite the fact that there are no oxygen atoms in this compound; therefore, this peak must be attributed to a transition from a molecular orbital composed of sulfur and zinc atoms. This molecular orbital could be composed of the *Zn*3d and *S*3p atomic orbitals, because their energies are very similar (around 8 eV), which favours the formation of the bond.

3.2.3. $K\beta'$ satellite line. In the anhydrite spectrum, a singular structure can be seen at the low energy side of the main peak (see figure 1(d)). It is known that this peak, usually referred to as $K\beta'$, corresponds to a transition from a molecular orbital composed of the *S*3p and *O*2s atomic orbitals [31]. On the other hand, as mentioned in section 3.2.1, the $K\beta_{1,3}$ line is related to a transition from a molecular orbital formed by the *S*3p and *O*2p orbitals. Then, the difference between both transitions is mainly due to the orbital of the ligand oxygen atom; thus, the energy difference between the $K\beta_{1,3}$ and $K\beta'$ lines (ΔE) can be related to the difference between the absorption edges *O*2p and *O*2s:

$$\Delta E = E(K\beta_{1,3}) - E(K\beta') \simeq E(O2p) - E(O2s). \quad (4)$$

This approximation works well if the orbitals of the ligand oxygen atom contribute in similar extents to both molecular orbitals. The energy difference ΔE obtained in this work was 14.0 ± 0.2 eV (see table 3) which is in good agreement with data from the literature for other sulfates [31].

3.2.4. $K\beta^{III}$ and $K\beta^{IV}$ satellite lines. The $K\beta^{III}$ and $K\beta^{IV}$ satellite lines were clearly observed in pure sulfur (S^0) and sphalerite (S^{-2}) (see figures 1(b) and (c)). The energy shifts of the $K\beta^{III,IV}$ doublet with respect to the $K\beta_{1,3}$ main peak are very close between these two samples: 2.5032 ± 0.0003 and 2.5044 ± 0.0005 keV for pure sulfur and sphalerite, respectively. This result was expected because these satellite lines are due to the presence of a *S*2p spectator hole, which is not significantly influenced by the chemical environment.

Due to the scarcity of data available for $K\beta^{III,IV}/K\beta$ intensity ratios, the results obtained in a previous work [38] were compared with the $K\alpha_{3,4}/K\alpha$ ratios determined in another previous work [37]. Making the rough assumption that the $K\alpha$ and $K\beta$ emission probabilities are unaffected by the presence of a 2p spectator hole, the comparison makes sense for a qualitative analysis. In both cases, a decrease of the intensity ratio with the atomic number was observed. Nevertheless, it was found that the values for $K\beta^{III,IV}/K\beta$ were systematically above the $K\alpha_{3,4}/K\alpha$ ratios. This behaviour is also observed here for pure sulfur: $K\alpha_{3,4}/K\alpha = 0.0502$ and $K\beta^{III,IV}/K\beta = 0.091$ (see tables 2 and 3). Therefore, the general behaviours of $K\beta^{III,IV}/K\beta$ and $K\alpha_{3,4}/K\alpha$ intensity ratios as functions of the atomic number are similar, but the assumption mentioned is not adequate for a quantitative comparison. In fact, a 2p spectator hole modifies the transition probability from the *L* shell in a greater extent than from an *M* shell. Particularly, it inhibits the decays from the *L* shell, resulting in a $K\alpha_{3,4}/K\alpha$ ratio lower than the corresponding $K\beta^{III,IV}/K\beta$ ratio.

3.2.5. $K\beta''$ satellite line. The $K\beta''$ line was detected only for anhydrite (see figure 1(d)). Its energy and relative intensity were determined from the spectral processing. The corresponding results are also shown in table 3. On the basis of theoretical calculations performed for sulfites [50], Torres Deluigi and Riveros [31] suggest that this transition can be attributed to the decay from a molecular orbital mainly composed of *O*2p, *S*3p and *S*3s atomic orbitals. On the other hand, for sulfates the theoretical spectra calculated by Uda *et al* [49] do not predict this transition because the presence of certain cations (for instance, Na^+ or K^+) bonded to the $(SO_4)^{2-}$ anion distorts the crystalline net. This fact shows

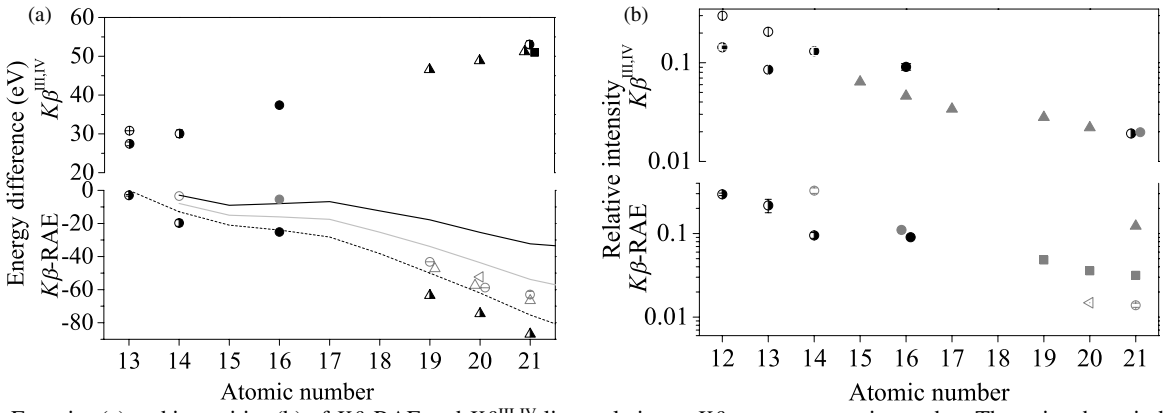

Figure 6. Energies (a) and intensities (b) of $K\beta$-RAE and $K\beta^{III,IV}$ lines relative to $K\beta_{1,3}$ versus atomic number. The point shape indicates the excitation source: electrons (circles), protons and heavy ions (squares) and photons (triangles), while their colour denotes the specific RAE transition: KM_1M_1 (black symbols), $KM_1M_{2,3}$ (grey open symbols) and $KM_{2,3}M_{2,3}$ (grey solid symbols). $E(K\beta^{III,IV})$: black solid circles: present results; right-half-filled circles: [38]; crossed circles: [5]; right-half-filled triangles: [1]; black solid squares: [2]. $E(K\beta$-RAE): black and grey solid circles: present results; black right-half-filled circles: [38]; black right-half-filled triangles: [1]; open grey circles: [38]; grey horizontal strikethrough circles: [20]; grey open up triangles: [1]; and grey open left triangle: [18]. Lines are related to the M-edge energies (see the text): $E(M_{2,3}) - 2E(M_1)$ (dashed line); $-E(M_1)$ (grey solid line); $-E(M_{2,3})$ (black solid line). $I(K\beta^{III,IV})$: grey symbols correspond to the experimental data of the $K\alpha_{3,4}$ intensity relative to the $K\alpha$ group. Black solid circles: present results; right half-filled circles: [38]; grey solid circles: [62]; vertical strikethrough circles: [6]; and grey solid triangles: [64]. $I(K\beta$-RAE): black and grey solid circles: present results; right half-filled circles: [38]; grey open circles: [38]; grey open triangle: [18]; grey solid triangles: [19]; grey solid squares: [23].

that it is necessary to consider, in the theoretical predictions, the C_{3v} symmetry of the sulfites, which is lower than the T_d symmetry of the sulfates.

The energy shift with respect to the main $K\beta_{1,3}$ line obtained here for calcium sulfate $\Delta E = 4.9$ eV (see table 3) agrees with the values obtained by Torres Deluigi and Riveros [31] for other sulfates.

The $K\beta''$ peak was also observed by other authors in several elements and with different interpretations. In the case of copper, for example, its origin is attributed to a modification of the atomic levels that arises by the presence of a 3d spectator hole [10, 12, 13, 68]. In titanium and chromium, some authors explain this transition by means of plasmon excitations [17]. Nevertheless, these explanations do not apply to sulfur due to its lack of 3d electrons in the ground state and its insulator character.

3.3. Comparison with other elements

Although this work is focused in the study of sulfur x-ray spectra, it is of interest to take advantage of the present measurements to compare with the behaviour followed by other elements. To this end, the energies and intensities of pure sulfur satellite lines in the $K\alpha$ and $K\beta$ regions are plotted in figures 5 and 6, respectively, along with results previously published and compiled in [37, 38], as functions of the atomic number. As can be seen, the energies and intensities obtained here (for $Z = 16$) follow the expected behaviour, on the basis of the previous results.

It can be noticed that no data were found in the region between silicon and potassium for pure elements, except for $K\alpha_{3,4}$. The results obtained here for sulfur may be useful for the interpolation of data for elements difficult to measure in the pure state in this region such as chlorine and argon.

4. Conclusion

The emission of x-rays in atomic transitions to the K shell of sulfur was studied in samples of pure sulfur, sphalerite and anhydrite. The creation of hole atomic states was induced by electron impact and the outgoing x-rays were registered with a wavelength dispersive system. A careful spectral analysis was performed by means of an in-house software previously developed. Characteristic line energies and RTP were determined as a result of the spectral processing.

Results of 13 transitions in pure sulfur (8 in the $K\alpha$ and 5 in the $K\beta$ spectral regions), 11 transitions in sphalerite (6 in the $K\alpha$ and 5 in the $K\beta$ groups) and 10 transitions in anhydrite (6 for $K\alpha$ and 4 for $K\beta$) were obtained. To our knowledge, no previous information can be found in the literature about the $K\alpha_{5,6}$ and $K\beta$ satellite lines for pure sulfur and no experimental data about the $K\beta_x$ line for S^{-2}.

The spectral features more sensitive with the oxidation state were the energy of the $K\alpha_1$ line, with shifts of -0.5 eV for sphalerite and $+0.8$ eV for anhydrite with respect to pure sulfur; the $K\alpha_3/K\alpha_4$ intensity ratio, with values of 1.26, 2.20 and 1.78, for sphalerite, pure sulfur and anhydrite, respectively; and the presence of the $K\beta'$ line, clearly notable in sphalerite and not appreciable in anhydrite and pure sulfur. These sensitive spectral features can be useful as tools for the analysis of sulfur oxidation states in materials characterization.

The $K\beta_{1,3}$ line of pure sulfur showed the internal structure previously observed by other authors, and consisting in two peaks of similar intensities. The energies and intensities of both peaks were determined through the spectral processing. This structure was not presented by the sphalerite and anhydrite.

The results of experimental studies about the x-ray emission from atoms in different oxidation states are useful to test theoretical models that attempt to describe effects of intra-atomic electron correlation, excitation and relaxation dynamics, etc. In the present case, the structure of K line

emission spectra was studied experimentally for sulfur in three oxidation states. Fine spectral features were characterized through the specific software developed, which allows us to describe the spectra in detail and to obtain magnitudes of physical interest.

Acknowledgment

The authors gratefully acknowledge Laboratorio de Microscopía Electrónica y Microanálisis of the Universidad Nacional de San Luis, Argentina, where measurements were carried out.

References

[1] Raju S S, Seetharami Reddy B, Murti M V R and Mombasawala L 2007 *X-Ray Spectrom.* **36** 35
[2] Hodge B, Kauffman R, Moore C F and Richard P 1973 *J. Phys. B: At. Mol. Phys.* **6** 2468
[3] Kavčič M, Budnar M, Mühleisen A and Török I 1998 *Nucl. Instrum. Methods* B **136** 173
[4] Uršič M, Kavčič M and Budnar M 2003 *Nucl. Instrum. Methods* B **211** 7
[5] Fischer D and Baun W 1965 *J. Appl. Phys.* **36** 534
[6] Keski-Rahkonen O, Mikkola E, Reinikainen K and Lehkonen M 1985 *J. Phys. C: Solid State Phys.* **18** 2961
[7] Mauron O and Dousse J-Cl 2002 *Phys. Rev.* A **66** 042713
[8] Soni S N 1996 *J. Phys. Chem. Solids* **57** 1831
[9] Bearden J A and Shaw C H 1935 *Phys. Rev.* **48** 18
[10] Deutsch M, Hölzer G, Härtwig J, Wolf J, Fritsch M and Förster E 1995 *Phys. Rev.* A **51** 283
[11] Song Y-F, Lee S-B and Chang Ch-N 1995 *Chin. J. Phys.* **33** 671
[12] Enkisch H, Sternemann C, Paulus M, Volmer M and Schülke W 2004 *Phys. Rev.* A **70** 022508
[13] Deutsch M, Förster E, Hölzer G, Härtwig J, Hämäläinen K, Kao C-C, Huotari S and Diamant R 2004 *J. Res. Natl Inst. Stand. Technol.* **109** 75
[14] Tsutsumi K, Nakamori H and Ichikawa K 1976 *Phys. Rev.* B **13** 929
[15] Srivastava K S, Singh S, Srivastava A K, Nayal R S, Chaubey A and Gupta P 1982 *Phys. Rev.* A **25** 2838
[16] Koster A S and Mendel H 1970 *J. Phys. Chem. Solids* **31** 2511
[17] Gokhale B G, Rai S and Rai S D 1977 *J. Phys. F: Met. Phys.* **7** 299
[18] Verma H 2000 *J. Phys. B: At. Mol. Opt. Phys.* **33** 3407
[19] Margeter E, Wegscheider W and Müller K 1984 *X-Ray Spectrom.* **13** 78
[20] Ford O 1932 *Phys. Rev.* **41** 577
[21] Servomaa A and Keski-Rahkonen O 1975 *J. Phys. C: Solid State Phys.* **8** 4124
[22] Keski-Rahkonen O and Ahopelto J 1980 *J. Phys. C: Solid State Phys.* **13** 471
[23] Johansson S A E, Campbell J L and Malmqvist K G 1995 *Particle Induced X-Ray Emission Spectrometry PIXE* (New York: Wiley) p 34
[24] Bé M, Lépy M, Plagnard J and Duchemin B 1998 *Appl. Radiat. Isot.* **49** 1367
[25] Maskil N and Deutsch M 1988 *Phys. Rev.* A **38** 3467
[26] Cipolla S J 1999 *Nucl. Instrum. Methods* A **422** 546
[27] Herren Ch and Dousse J-Cl 1997 *Phys. Rev.* A **56** 2750
[28] Urch D 1970 *J. Phys. C: Solid State Phys.* **3** 1275
[29] Urch D 1985 X-ray spectroscopy and chemical bonding in minerals *Chemical Bonding and Spectroscopy in Mineral Chemistry* ed F J Berry and D J Vaughan (London: Chapman and Hall) p 31
[30] Gysels K, Deutsch F and Van Grieken R 2002 *Atmos. Environ.* **36** 4103
[31] Torres Deluigi M and Riveros J 2006 *Chem. Phys.* **325** 472
[32] Torres Deluigi M, Perino E, Olsina R and Riveros de la Vega A 2003 *Spectrochim. Acta* B **58** 1699
[33] Peng G *et al* 1994 *J. Am. Chem. Soc.* **116** 2914
[34] Limandri S, Ceppi S, Tirao G, Stutz G, Sánchez C and Riveros J 2010 *Chem. Phys.* **367** 93
[35] Kawai J, Takami M and Satoko C 1990 *Phys. Rev. Lett.* **65** 2193
[36] Rowe M, Kent A and Nielsen R 2007 *Chem. Geol.* **236** 303
[37] Limandri S, Bonetto R, Carreras A and Trincavelli J 2010 *Phys. Rev.* A **82** 032505
[38] Limandri S, Carreras A, Bonetto R and Trincavelli J 2010 *Phys. Rev.* A **81** 012504
[39] Słabkowska K and Polasik M 2003 *Nucl. Instrum. Methods* B **205** 123
[40] Anagnostopoulos D F, Borchert G, Gotta D, Rashid K, Jakubassa-Amundsen D H and Amundsen P A 1998 *Phys. Rev.* A **58** 2797
[41] Mauron O, Dousse J-Cl, Hoszowska J, Marques J P, Parente F and Polasik M 2000 *Phys. Rev.* A **62** 062508
[42] Nishikida S and Ikeda S 1978 *Bull. Chem. Soc. Japan* **51** 1996
[43] Soni S N 1997 *Phys. Lett.* A **237** 48
[44] Kavčič M, Karydas A G and Zarkadas Ch 2004 *Nucl. Instrum. Methods* B **222** 601
[45] Harrison R M and Van Grieken R E (ed) 1998 *Atmospheric Particles (IUPAC Series on Analytical and Physical Chemistry of Environmental Systems* vol 5*)* (Chichester: Wiley)
[46] Chuang C C, Penner J E, Taylor K E, Grossman A S and Walton J J 1997 *J. Geophys. Res.* **102** 3761
[47] Carrol M and Rutherford M 1988 *Am. Mineral.* **73** 845
[48] Kavčič M, Dousse J, Szlachetko J and Cao W 2007 *Nucl. Instrum. Methods* B **260** 642
[49] Uda E, Kawai J and Uda M 1993 *Nucl. Instrum. Methods Phys. Res.* B **75** 24
[50] Mogi M, Ota A, Ebihara S, Tachibana M and Uda M 1993 *Nucl. Instrum. Methods Phys. Res.* B **75** 20
[51] Bonetto R, Castellano G and Trincavelli J 2001 *X-Ray Spectrom.* **30** 313
[52] Limandri S P, Trincavelli J C, Bonetto R D and Carreras A C 2008 *Phys. Rev.* A **78** 022518
[53] Bearden J A 1967 *Rev. Mod. Phys.* **39** 78
[54] Trincavelli J and Castellano G 2008 *Spectrochim. Acta* B **63** 1
[55] Trincavelli J, Limandri S, Carreras A and Bonetto R 2008 *Microsc. Microanal.* **14** 306
[56] Limandri S P, Bonetto R D, Di Rocco H O and Trincavelli J C 2008 *Spectrochim. Acta* B **63** 962
[57] Scofield J H 1974 *Phys. Rev.* A **9** 1041
[58] Wallace P J and Carmichael I S E 1994 *Am. Mineral.* **79** 161
[59] Tada T, Fukuda H, Hasegawa J and Oguri Y 2010 *Spectrochim. Acta* B **65** 46
[60] Alonso Mori R, Paris E, Giuli G, Eeckhout S G, Kavčič M, Žitnik M, Bučar K, Petterson L G M and Glatzel P 2009 *Anal. Chem.* **81** 65
[61] Nigam A N and Soni S N 1980 *J. Phys. C: Solid State Phys.* **13** 1567
[62] Parratt L G 1936 *Phys. Rev.* **50** 1
[63] Yokoi K, Oohashi H, Ito Y, Tochio T and Shoji T 2006 *Radiat. Phys. Chem.* **75** 1461

[64] Babu G R, Gopalakrishna V, Raju M L N, Parthasaradhi K, Murty V R K, Murti M V R and Rao K S 1987 *Phys. Rev.* A **36** 386
[65] Alonso Mori R, Paris E, Giuli G, Eeckhout S G, Kavčič M, Žitnik M, Bučar K, Petterson L G M and Glatzel P 2010 *Inorg. Chem.* **49** 6468
[66] Chung M F and Jenkins L H 1970 *Surf. Sci.* **22** 479
[67] Sevier K D 1972 *Low Energy Electron Spectrometry* (New York: Wiley-Interscience)
[68] LaVilla R E 1979 *Phys. Rev.* A **19** 717
[69] Knudson A R, Nagel D J, Burkhalter P G and Dunning K L 1971 *Phys. Rev. Lett.* **26** 1149
[70] Jamison K A, Woods C W, Kauffman R L and Richard P 1975 *Phys. Rev.* A **11** 505
[71] Török I, Papp T and Raman S 1999 *Nucl. Instrum. Methods* B **150** 8
[72] Deutsch M 1989 *Phys. Rev.* A **39** 3956
[73] Graeffe G, Juslén H and Karras M 1977 *J. Phys. B: At. Mol. Phys.* **10** 3219
[74] Mauron O and Dousse J-Cl 2002 *Phys. Rev.* A **66** 042713
[75] Salem S I and Scott B L 1987 *Phys. Rev.* A **35** 1607
[76] Kavčič M 2003 *Phys. Rev.* A **68** 022713